Heliyon 5 (2019) e01955

Contents lists available at ScienceDirect

Heliyon

journal homepage: www.heliyon.com

Doxorubicin loaded carboxymethyl Assam bora rice starch coated superparamagnetic iron oxide nanoparticles as potential antitumor cargo

Sharmistha Mohapatra [a,b,**], Mohammed Asfer [c], Mohammed Anwar [b], Kalicharan Sharma [a], Mymoona Akhter [a], Farhan Jalees Ahmad [b], Anees Ahmad Siddiqui [a,*]

[a] Department of Pharmaceutical Chemistry, School of Pharmaceutical Education and Research, Jamia Hamdard, New Delhi, India
[b] Nanoformulation Research Laboratory, School of Pharmaceutical Education and Research, Jamia Hamdard, New Delhi, India
[c] Department of Mechanical Engineering, College of Engineering, Dawadmi Shaqra University, Saudi Arabia

ARTICLE INFO

Keywords:
Pharmaceutical chemistry
Carboxymethylation
Assam bora-rice starch
Doxorubicin hydrochloride
Molecular docking
MTT assay

ABSTRACT

In recent years, polysaccharide-decorated superparamagnetic iron oxide nanoparticles (SPIONs) have gained attention in the field of "nanotheranostics" with integrated diagnostic and therapeutic functions. Carboxymethyl Assam bora rice starch-stabilized SPIONs (CM-ABRS SPIONs), synthesized by co-precipitation method, has already shown exciting potential towards magnetic drug targeting potential. After establishing it as a promisable targeting carrier, the present study is focused on the next step i.e. to evaluate its *In vitro* anti-tumor potential by loading anticancer drug "Doxorubicin hydrochloride (DOX)" onto CM-ABRS SPIONs. DOX-loaded CM-ABRS SPIONs were physico-chemically characterized by DLS, zeta-potential, TEM, FT-IR, XRD, and VSM analysis. Spectroflourimetric analysis confirmed the maximum loading of DOX up to 6% (w/w) onto CM-ABRS SPIONs via electrostatic interactions. Further, molecular level drug performance was investigated by docking study against receptors (HER-2 and Folate receptor-α) over expressed in cancer cells and MTT assay (in MCF-7 and HeLa cell line), which conferred promisable results of DOX-CM-ABRS SPIONs as compared to standard DOX solution.

1. Introduction

In the field of biomedical research, nanoparticles (NPs) with controlled drug release properties are being explored to overcome the shortcomings (relative non-specificity and potential side effects to healthy tissues) of conventional therapeutics. Their potential use as "nanotheranostics" with integrated diagnostic and therapeutic functions offers opportunities for novel therapy of complex disorders such as cancer, inflammatory and neurodegenerative diseases (Lammers et al., 2010). Specifically, theranostic metallic nanoparticles (TMNPs) between the molecular (~10 nm) and bulk (~200 nm) size range with particular functional groups, have gained much scientific interest to overcome the biological barriers to drug delivery. Among various types of TMNPs, super-paramagnetic iron oxide nanoparticles (SPIONs) consisting of ~15 nm iron oxide core (magnetite (Fe_3O_4) or maghemite (γ-Fe_2O_3)) have been found to possess unique electronic, optical and magnetic properties, which can be attributed to their high surface-to-volume ratio (Xie et al., 2009). These unique properties make SPIONs an excellent candidate for surface engineering and functionalization to improve drug payload and drug performance with low immunogenicity and fewer side effects associated with drug delivery system (Arruebo et al., 2007; Fang et al., 2009; Lammers et al., 2010; Veiseh et al., 2010). Also, SPIONs gained the primary choice for delivery of anticancer drugs, due to their feasibility to localize at the target site upon the application of an external magnetic field, thus improving the therapeutic efficacy of the drug (Laurent et al., 2014; Reyes-Ortega et al., 2017). SPIONs, being biocompatible in nature, are being used for various biomedical applications as: (i) contrast agents for high-resolution magnetic resonance imaging (MRI) and (ii) promising therapeutic cargo for delivering and maintaining drug concentration at target site (Corot et al., 2006; Shubayev, Pisanic II & Jin, 2009). Pre-clinically and clinically, various natural and synthetic biodegradable polymers have been studied to impart "stealthness" and prolonging plasma circulation of SPIONs to maximize the likelihood of reaching targeted tissues in controlled and sustained release manner with enhanced accumulation at the tumor site via the enhanced permeability and retention (EPR) effect (Cheng et al., 2009; Park et al., 2008; Wang

* Corresponding author.
** Co-corresponding author.
E-mail addresses: sharmistha.mhptr@gmail.com (S. Mohapatra), prof.anees1@gmail.com (A.A. Siddiqui).

https://doi.org/10.1016/j.heliyon.2019.e01955
Received 14 January 2019; Received in revised form 30 April 2019; Accepted 12 June 2019

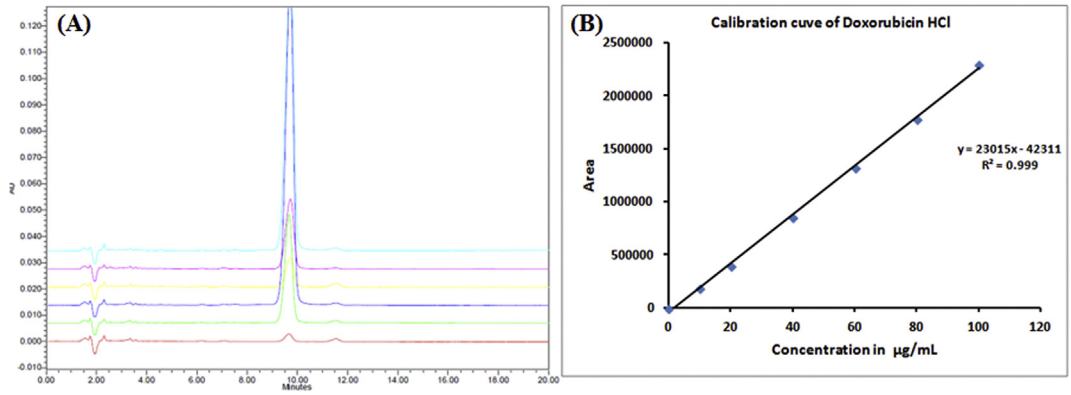

Fig. 1. (A) Overlay HPLC chromatogram of DOX at different concentration levels, and (B) Standard calibration plot of DOX.

et al., 2015; Xu et al., 2017; Zhang et al., 2018a). Being made of biodegradable, hydrophilic and controlled released polymer, carboxymethyl starch (CMS) has also been investigated extensively as a coating agent for SPIONs to achieve stable, spherical and relatively mono-disperse particles for drug delivery with improved drug tolerance, and/or better drug bioavailability (Saboktakin et al., 2009; Tang et al., 2019). They have also been demonstrated as contrast agents for cancer diagnosis (Kim et al., 2003).

In the present study, carboxymethyl Assam Bora rice starch (CM-ABRS) has been utilized for SPIONs stabilization and further it's ability to effectively bind and loadd cationic anti-cancer drug molecule, Doxorubicin hydrochloride (DOX), via electrostatic interaction (Wang et al., 2015; Zhang et al., 2018b), has been demonstrated. DOX, being a hydroxy derivative of anthracycline class chemotherapeutic, is widely applied to treat leukaemia, ovarian cancer and especially late-stage breast cancer (Chen et al., 2017; Hoke et al., 2005). In order to minimize undesired interaction of DOX into healthy tissues, a biodegradable and targetable nanocarrier has been developed, wherein the amount and site of drug release is controlled by the surface engineering and pH of the medium (Akbarzadeh et al., 2012). There is recent growing interest in polyelectrolyte complexes (PEC) prepared via electrostatic interactions between oppositely-charged polymers and/or drug molecules in an aqueous medium due to their easy preparation protocol under mild and non-toxic conditions (Meka et al., 2017). This ideal strategy is already reported to encapsulate and deliver cationic drugs viz; epirubicin (Zhang et al., 2015), 5-aminosalicylic acid (mesalamine) (Saboktakin et al., 2009) and multinuclear platinum (II) drugs (Xiao et al., 2013) with no chemical modifications to increase bioavailability while maintaining or enhancing efficacy.

To the best our knowledge, from literature survey, it is our first attempt to utilize the inherent properties of CM-ABRS to explore its potential as a stabilizing agent for SPIONs and a cargo for loading anticancer drug molecule, DOX, via electrostatic interaction for establishing a promisable carrier for anticancer drug delivery.

2. Materials and methods

2.1. Materials

Ferric chloride anhydrous ($FeCl_3$) and ferrous sulphate heptahydrate ($FeSO_4.7H_2O$) were procured from Fluka Chemicals, India. Assam Bora rice was obtained from local villagers of Dibrugarh district of upper Assam, India. Ammonium hydroxide (25% (v/v)), monochloro acetic acid, glacial acetic acid, and sodium hydroxide flakes (NaOH) were purchased from S.D. fine chem. Ltd., Mumbai, India. DOX was kindly gifted by United Biotech, Delhi, India. Double distilled water (DDW), prepared in the laboratory, was used for all the experiments. All other chemicals used in the experiment were of analytical reagent grade and used without further purification.

2.2. HPLC method for DOX

HPLC analysis of DOX was performed with a Waters e 2695 Separations Module HPLC system (Waters Corporation, USA) connected to an autosampler, and a Waters 2998 Photodiode Array (PDA) Detector as per British pharmacopeia (Pharmacopoeia, 1999). Stationary phase comprised of Hypersil™ C_{18} ODS (150 × 4.6 mm; 5 µm, Thermo Fischer Scientific Inc., USA) column, operated at ambient temperature. Mobile phase consisted of solution A and solution B (1:1 ratio), where solution A comprised of 5 parts of methanol and 45 parts of acetonitrile, and solution B comprised of 2.88 g L^{-1} of sodium lauryl sulfate and 2.30 g L^{-1} of phosphoric acid in water. Mobile phase was pumped at a flow rate of 1 mL min^{-1} with a detection wavelength of 480 nm. Ten microliters of sample solution was injected in each run with a total chromatographic run time of 20.0 min. All samples were passed through a 0.22-µm syringe filter prior to HPLC analysis. Data acquisition, data handling, and instrument control were performed by Empower® software v 2.0.

2.2.1. Preparation of stock solution and calibration standard samples

Stock solution of DOX (1000 µg mL^{-1}) was prepared by dissolving 5 mg of drug in 5 mL of HPLC-grade water and stored at 4°C for future use. The working standard solutions of DOX at different concentrations were prepared separately by diluting the stock solutions in HPLC-grade water and were prepared fresh daily prior to analysis. The peak area of each concentration was plotted against the corresponding concentration to obtain the calibration graph of DOX.

2.3. Preparation of DOX-CM-ABRS SPIONs

2.3.1. Synthesis of CM-ABRS

Assam Bora rice starch (ABRS) was extracted from native Assam Bora rice (grains of *Oryza sativa*, family Gramineae) as per previously described method (Ahmad et al., 2012). Briefly, ABRS was dispersed in iso-propanol and treated with alkali (8N) in presence of chloroacetic acid (etherifying agent) at 65°C with optimum stirring (~2000 rpm) to synthesize carboxymethyl Assam Bora rice starch (CM-ABRS) based on Williamson's ether synthesis. The optimized sample of CM-ABRS was neutralized with glacial acetic acid (50% (v/v)) and purified by filtration and washing with ethanol (85% (v/v)) until the pH of the liquid was neutral (pH = 7), as described in our previous work (Mohapatra et al., 2017).

2.3.2. Synthesis of CM-ABRS SPIONs

Carboxymethyl Assam Bora rice starch coated SPIONs (CM-ABRS SPIONs) were synthesized chemically by co-precipitation reaction from an aqueous mixture of ferrous and ferric salts (1:2 M ratio) with varying concentrations of CM-ABRS solution (0.1–1.0% (w/v) in alkaline medium at 70–75°C in an inert nitrogen atmosphere with continuous stirring. Then, the prepared CM-ABRS SPIONs were passed through a

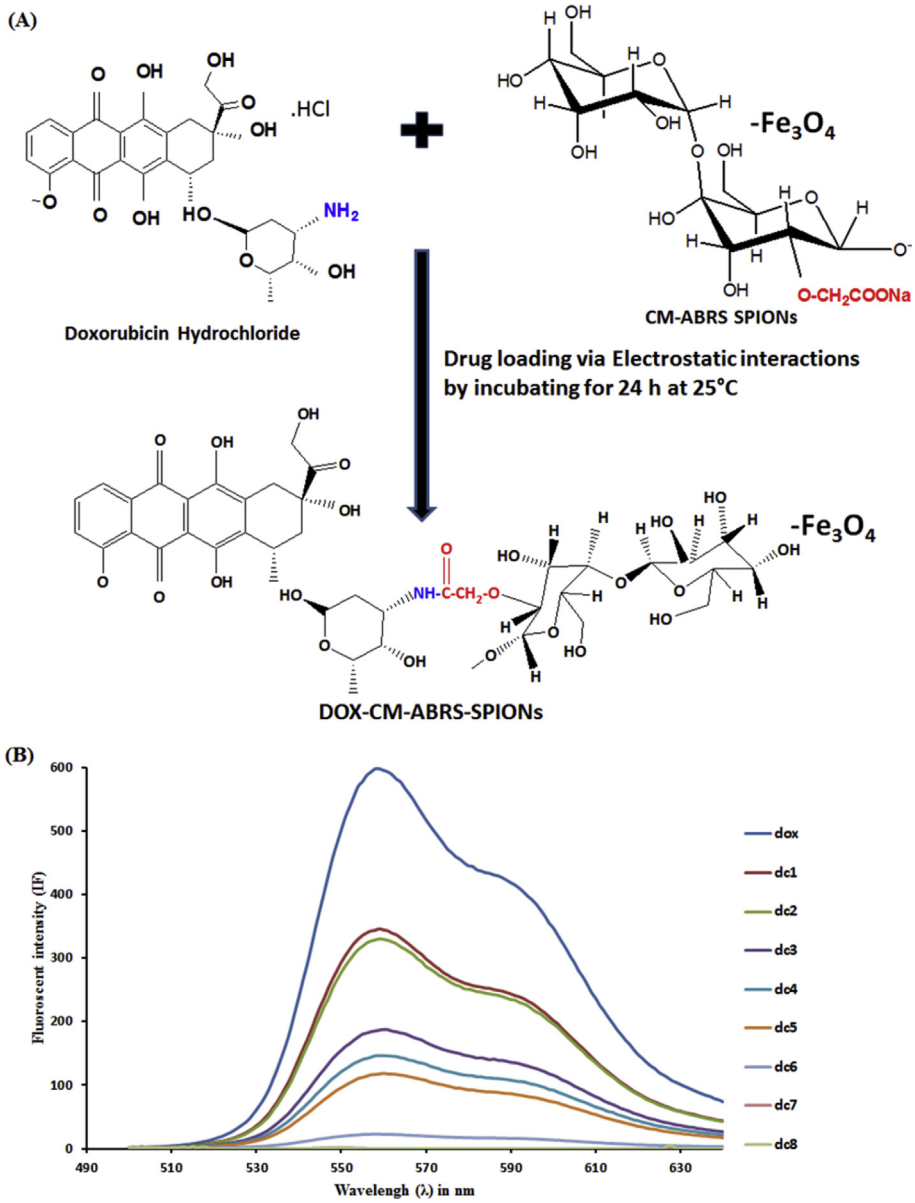

Fig. 2. (A) Schematic representation of probable complex formed between DOX and CM-ABRS (0.8% (w/v)) SPIONs, and (B) Fluorescence spectra of DOX solution (120 μg/4.5 mL DDW) incubated with increasing amounts of CM-ABRS (0.8% (w/v)) SPIONs (0.25 mg; dc1) (0.50 mg; dc2) (0.75 mg; dc3) (1.0 mg; dc4) (1.5 mg; dc5) (1.75 mg; dc6) (2.0 mg; dc7) (2.5 mg; dc8), respectively.

homogenizer (Silent Crusher S, Heidolph Instruments GmbH & Co. KG) at different homogenization speeds and cycles to get more uniform small-sized particles. Effect of concentration of capping agent (polymer: CM-ABRS) and process variables of homogenization (speed and cycles) on average particle size (Z-average) and polydispersity index (PDI) were investigated to get an optimum particle size range for CM-ABRS (0.8% (w/v)) SPIONs, as discussed briefly in our previous work (Mohapatra et al., 2018).

$$Fe^{2+} + 2Fe^{3+} + CM - ABRS + 8OH^- \xrightarrow{\substack{alkaline\ pH\ ,75^{\circ}C;\\ inert\ atmosphere}} CM - ABRS - Fe_3O_4 + 4H_2O \quad (1)$$

2.3.3. DOX loading onto CM-ABRS SPIONs

In order to determine the drug loading efficiency, a predetermined amount of DOX solution (120 μg/4.5 mL DDW) was added serially to increasing amounts of lyophilized CM-ABRS (0.8% (w/v)) SPIONs without mannitol: 0.25 mg (dc1), 0.50 mg (dc2), 0.75 mg (dc3), 1.0 mg (dc4), 1.5 mg (dc5), 1.75 mg (dc6), 2.0 mg (dc7), 2.5 mg (dc8). Incubator shaker (Shel Lab, USA) at 150 rpm was used to incubate all the samples for 24 h at 25 °C. The maximum amount of DOX loading in CM-ABRS (0.8% (w/v)) SPIONs was determined by observing the fluorescence quenching of DOX, which was monitored at an excitation wavelength of 480 nm and emission wavelength range of 500–640 nm, on a RF-5301 PC spectrofluorometer (Shimadzu, Japan). Photodegradation of DOX was prevented by conducting all experiments in dark. Finally, the incubated sample showing optimum quenching (maximum drug loading) was lyophilized (Labconco, USA) to get completely dry sample of DOX-CM-ABRS (0.8% (w/v)) SPIONs.

$$CM - ABRS - Fe_3O_4 + DOX \xrightarrow{Incubation/24\,h,25^{\circ}C} DOX - CM - ABRS - Fe_3O_4 \quad (2)$$

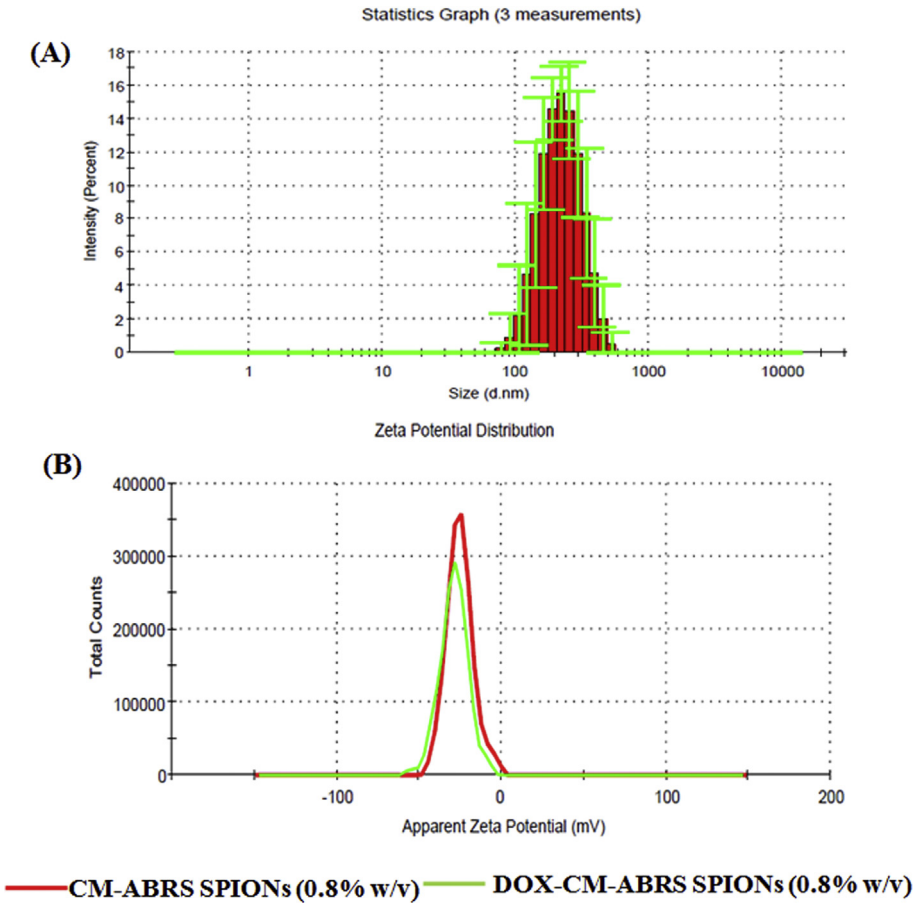

Fig. 3. Particle size distribution of (A) DOX-CM-ABRS (0.8% (w/v)) SPIONs, and (B) comparative zeta potential distribution curves of CM-ABRS (0.8% (w/v)) SPIONs and DOX-CM-ABRS (0.8% (w/v)) SPIONs.

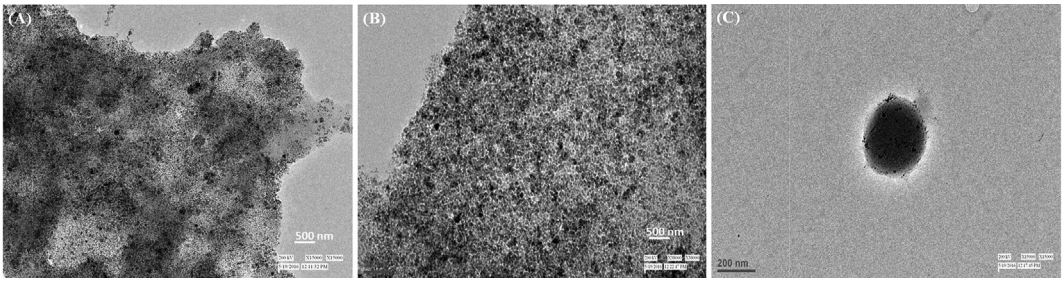

Fig. 4. TEM micrograph of (A) CM-ABRS (0.8% (w/v)) SPIONs (B) DOX-CM-ABRS (0.8% (w/v)) SPIONs and (C) Single cluster entrapping multiple iron oxide cores.

2.3.3.1. Estimation of drug loading and entrapment efficiency. For determining drug loading and entrapment efficiency, the lyophilized DOX-CM-ABRS (0.8% (w/v)) SPIONs were first dissolved in DMSO/water (1/9 (v/v)). The fluorescence spectra of the supernatant obtained was recorded by using RF-5301 PC spectrofluorometer (Shimadzu, Japan), at an excitation wavelength of 480 nm and emission wavelength range of 500–640 nm. Entrapment efficiency (EE, wt %) and loading capacity (DL, wt %), were calculated according to the following formulae, in triplicate:

$$\boldsymbol{EE}\ (\%) = \frac{\boldsymbol{W_f}}{\boldsymbol{W_i}} \times \mathbf{100} \tag{3}$$

$$\boldsymbol{DL}\ (\%) = \frac{\boldsymbol{W_f}}{\boldsymbol{W_t}} \times \mathbf{100} \tag{4}$$

Where, W_i, W_f, and W_t stand for the total weight of the added DOX, weight of loaded DOX and the total weight of formulation (DOX-CM-ABRS (0.8% (w/v)) SPIONs) taken.

2.4. Physicochemical characterization of DOX-CM-ABRS SPIONs

2.4.1. Particle size, size distribution and surface charge: DLS analysis

The hydrodynamic size (Z-average) and polydispersity index (PDI) of CM-ABRS (0.8% (w/v)) SPIONs and DOX-CM-ABRS (0.8% (w/v)) SPIONs were recorded by using dynamic light scattering (DLS) measurements, using Zetasizer instrument (Nano ZS, Malvern Instruments, Malvern, UK). The same instrument was used to measure the surface charge (zeta potential) of the formulations. Prior to analysis, all the samples were diluted with nitrogen-purged DDW and ultra-sonicated for 10–15 min. All measurements were performed in triplicate at 25 °C at a

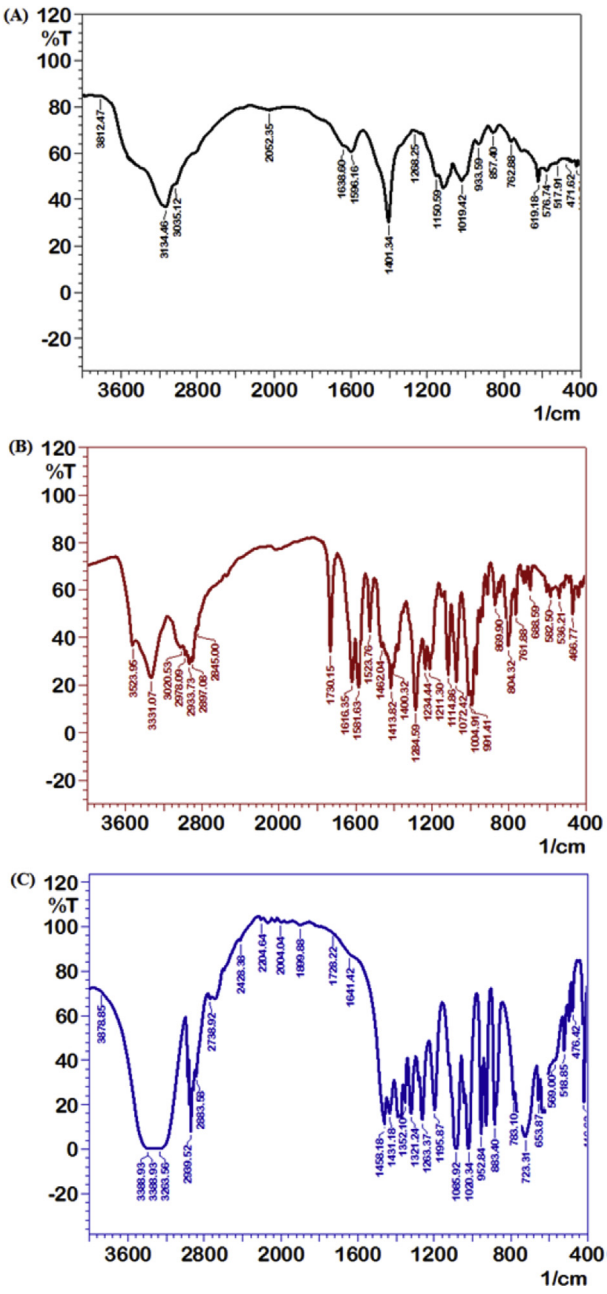

Fig. 5. FT-IR spectra of (A) CM-ABRS (0.8% (w/v)) SPIONs (B) DOX, and (C) DOX-CM-ABRS (0.8% (w/v)) SPIONs.

detection angle of 90°.

2.4.2. Particle morphology: transmission electron microscopy (TEM)

Size and morphology of CM-ABRS (0.8% (w/v)) SPIONs and DOX-CM-ABRS (0.8% (w/v)) SPIONs were illustrated by transmission electron microscopy (TEM). The samples for TEM detection were prepared by putting a drop of sample solution on a carbon-coated copper grid after ultrasonication, and then drying it at room temperature, followed by TEM viewing using HR-TEM instrument (TECNAI G^2 (200 kV), FEI, Holland).

2.4.3. Interaction of CM-ABRS SPIONs with DOX: fourier-transform infrared (FT-IR) spectroscopy

The nature of interaction between DOX and CM-ABRS SPIONs was confirmed by FT-IR spectrophotometer (IR affinity-1, Shimadzu, Japan). The FT-IR spectra were recorded in the range of 4000–400 cm^{-1} at a resolution of 4 cm^{-1} on samples finely grinded and dispersed in KBr

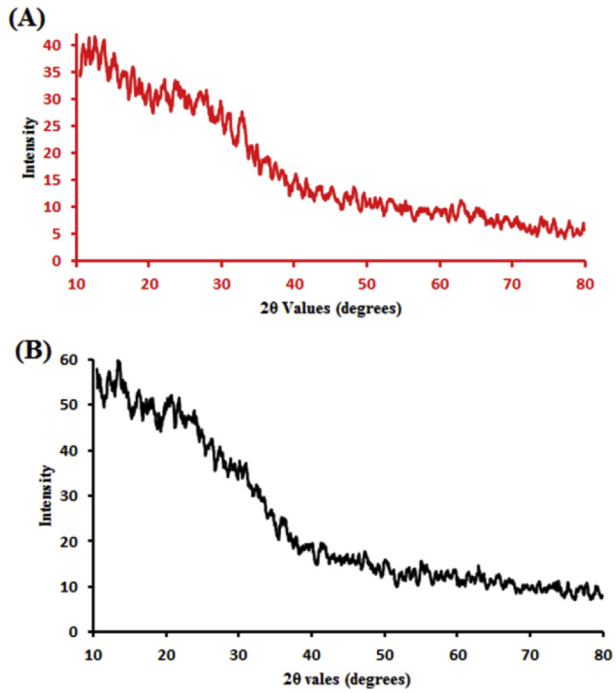

Fig. 6. X-ray diffractogram of (A) CM-ABRS (0.8% (w/v)) SPIONs, and (B) DOX-CM-ABRS (0.8% (w/v)) SPIONs.

pellet, under dry air at room temperature. The FT-IR spectra for CM-ABRS (0.8% (w/v)) SPIONs, DOX, and DOX-CM-ABRS (0.8% (w/v)) SPIONs were recorded after keeping the sample inside the instrument, in transmittance mode. Looking at the peak positions, functional groups were compared and characterized.

2.4.4. Crystallographic properties: X-ray diffraction analysis (XRD)

The physical form of the CM-ABRS (0.8% (w/v)) SPIONs and DOX-CM-ABRS (0.8% (w/v)) SPIONs were analyzed by using a Rigaku diffractometer (Rigaku, Japan) equipped with XG operation RINT2200 Target: Cu software for data acquisition and processing, over the 2θ range of 10°–80° at a rate of 8 min^{-1} with a step size of 0.02°, using Cu-Kα radiation (λ = 1.54060 A). The matching of peak positions and their relative intensities with reference JCPDS (Joint Committee on Powder Diffraction Standards) files, were done to confirm the crystallite phase of samples.

2.4.5. Magnetic properties measurement: vibrating sample magnetometry (VSM)

Vibrating sample magnetometry (VSM) (LDJ9600-1, LDJ, USA) was used to investigate the magnetic properties of CM-ABRS (0.8% (w/v)) SPIONs and DOX-CM-ABRS (0.8% (w/v)) SPIONs in the form of magnetization curves. Magnetic field was applied in the range of 0–18 kOe for this study. Micro Sense Easy VSM software was used for data acquisition and processing.

2.5. In silico drug design study: molecular docking

Modeling studies are required in order to construct molecular models that help in better understanding of binding mode of final formulation (DOX-CM-ABRS SPIONs) at the molecular level against Human epidermal receptor 2 (HER-2) at catalytic ligand binding site (PDBID: 5jeb) and FRA (Folate receptor-α), catalytic ligand binding site (PDBID: 4lrh), which are over expressed in several epithelial-derived tumors including ovarian, breast, renal, lung, colorectal and brain, for better understanding of the binding phenomenon at the molecular level. HER-2 is a family of receptors that plays a central role in the pathogenesis of

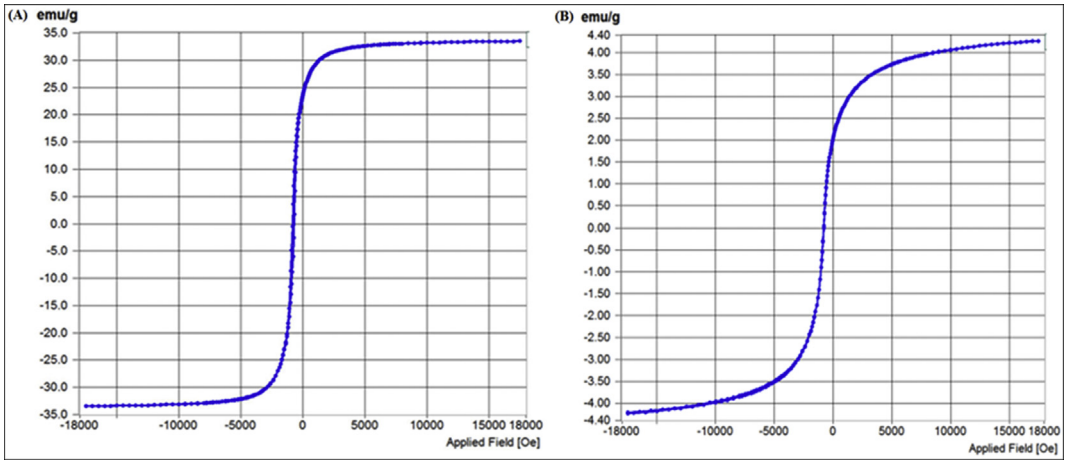

Fig. 7. VSM data showing the M–H curves for (A) CM-ABRS (0.8% (w/v)) SPIONs, and (B) DOX-CM-ABRS (0.8% (w/v)) SPIONs.

several human cancers. They regulate cell growth, survival, and differentiation via multiple signal transduction pathways and participate in cellular proliferation and differentiation. Hence, HER-2 receptors overexpressed in tumor cells act as an active target for various cancer therapeutics (Ménard et al., 2003; Neve et al., 2001; Olayioye, 2001). The docking study of DOX-CM-ABRS SPIONs against HER-2 and FRA receptors was performed using Maestro, version 9.6, implemented from Schrodinger software suite (Release, 2017). All the ligands were sketched in 3D format using build panel and were prepared for docking using ligprep application. The protein for docking study was taken from protein data bank (PDB ID: 5jeb) and prepared by removing solvent, adding hydrogen and further minimization in the presence of bound ligand (6JS) using protein preparation wizard. Grids for molecular docking were generated with bound co-crystallized ligand. For the validation of docking parameters the co-crystal ligand (6JS) was re-docked at the catalytic site of protein and if the RMSD (root mean square deviation) of the best docked conformation was found to be < 2.0 Å from the bound ligand in the experimental crystal, then the used scoring function was considered to be successful, as reported in literature (Paul and Mukhopadhyay, 2004). Therefore, the docked results were compared to the crystal structure of the bound ligand–protein complex. DOX-CM-ABRS SPIONs were docked using Glide extra-precision (XP) mode, with maximum of three poses saved per molecule (Friesner et al., 2006; Jones et al., 1997).

2.6. In vitro drug release profile

For the *In vitro* drug release study, a weighed amount of lyophilized DOX-CM-ABRS (0.8% (w/v)) SPIONs was suspended in 5 mL of phosphate buffered saline (PBS, pH 7.4) in a dialysis membrane (MWCO-10,000 Da, Sigma). Prior to use, the dialysis membrane (MWCO- 10,000 Da) was activated according to the protocol provided by Sigma and soaked in the release media (PBS, pH 7.4) overnight before sample loading. The dispersed samples (5 mL) were sealed in dialysis membrane and then incubated in the release media (50 mL) by placing in a shaking incubator (Shel Lab, USA) at 37 ± 2°C under mild agitation of 150 rpm. At pre-determined time intervals, the 2 mL of exterior solution was taken out and replaced with equal volume of fresh PBS. The percentage of DOX released was quantified by using HPLC method, after filtering through 0.22-μm nylon syringe filter. Each study was carried out in triplicate, and data presented as mean ± SD (standard deviation) (n = 3). Then, the release data was fitted into various kinetic models to find out the best release kinetics of the formulation (Guo et al., 2010).

2.7. In vitro cell viability assay

2.7.1. Cell lines

In vitro cell viability assay was carried out against human breast cancer (MCF-7) and cervical cancer (HeLa) cell lines. Cells were cultured in 75 cm^2 flask containing Dulbecco's Modified Eagle Medium (DMEM) supplemented with 10% (v/v) heat-inactivated fetal bovine serum (FBS) and 1% (v/v) antibiotic solution (100 U mL^{-1} of penicillin, 100 mg mL^{-1} streptomycin and 0.25 mg mL^{-1} amphotericin B); 10 mM HEPES (4-(2-hydroxyethyl)-1-piperazineethanesulfonic acid) and 25 mM sodium bicarbonate at 37°C in a humidified atmosphere of 5% CO_2 in air-jacketed incubator (NuAire, Inc., USA). Stock cultures of both cell lines were kept in the exponential growth phase by passaging as monolayer culture using 0.02% EDTA. For routine reseeding the dislodged cells were suspended in complete medium, as discussed above.

2.7.2. MTT assay

The cytotoxic effect at different concentrations of DOX (standard) and DOX-CM-ABRS (0.8% (w/v)) SPIONs (test) was assessed in both cell lines by the MTT assay method (Mallick et al., 2016). This test measures the number of metabolically-active, living cells that are able to transform the yellow product 3-(4, 5-dimethylthiazol-2-yl)-2,5-diphenyl tetrazolium bromide (MTT) into the blue formazan dye via mitochondrial reduction by succinate dehydrogenase (mitochondrial enzyme). To carry out the study, the cells were seeded overnight at 1×10^4 per well in a 96-welled flat-bottomed plates (Falcon Plate, Corning Costar, USA) and then incubated for a period of 24 h to allow cell adherence. After 24 h, growth media was removed from each well and 200 μL of media containing different concentrations (0.001, 0.01, 0.1, 1.0, 10, 100 μg mL^{-1}) of test and standard samples were added. Untreated cells containing CM-ABRS (0.8% (w/v)) SPIONs (placebo) were used as the control group. After an incubation period of 48 h, MTT in PBS (5 mg mL^{-1}, 20 μL) was added to each well reaching a final concentration of 0.5 mg mL^{-1} and again subjected to CO_2 incubator for 4 h, followed by removal of media. After 4 h, formazan crystals formed by mitochondrial reduction of MTT were solubilized in DMSO (150 μL/well) on a shaking plate for 5 min. Finally, the absorbance was recorded at 570 nm on the iMark Microplate Reader (Bio-Rad, USA) after 10 min incubation. Percentage cell viability was calculated with the following formula:

$$\%\ \textbf{growth inhibition} = \frac{\textit{OD test}}{\textit{OD control}} \times \mathbf{100} \quad (5)$$

Microsoft Excel 2007 software was used to calculate percent cell

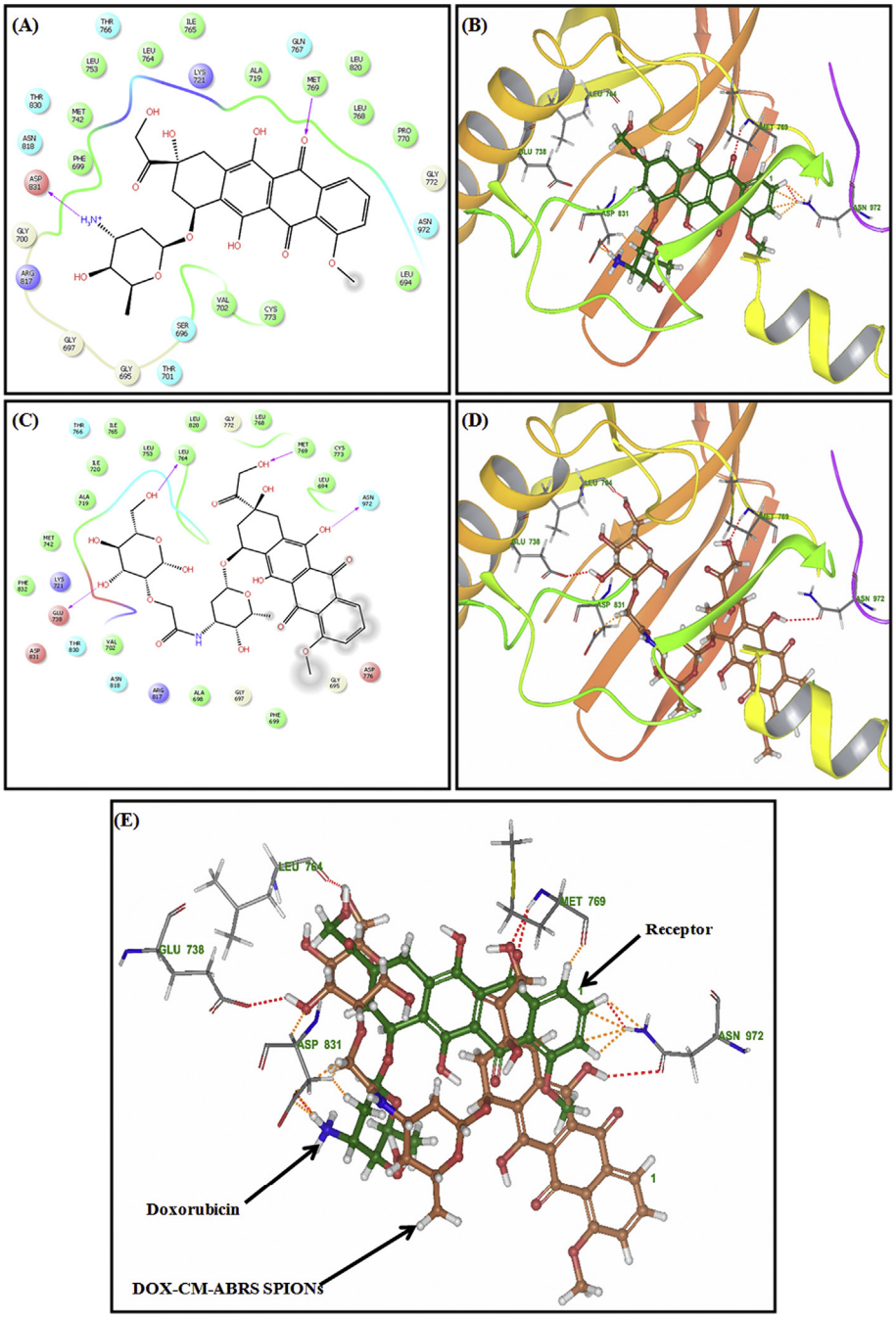

Fig. 8. Best conformations for compounds docked to HER-2 receptor (green color) (A) Ligplot of DOX (B) 3D plots showing binding sites of DOX (grey sticks) with the corresponding HER-2 receptor (C) Ligplot of DOX-CM-ABRS SPIONs (D) 3D plots showing binding sites of DOX-CM-ABRS SPIONs(grey sticks) with the corresponding HER-2 receptor, and (E) Superimposition of DOX-CM-ABRS SPIONs (brown) at catalytic domain of HER-2 receptor with DOX (blue).

viability, plot the survival (viability) curves and determine IC_{50} values. Also, dose-dependent and time-dependent cytotoxicity with the incubation period upto 72 h was also studied for DOX-CM-ABRS-SPIONs (0.8% (w/v)) in comparison to standard DOX solution.

2.8. Statistical analysis

All readings of the study were taken in triplicate and expressed as mean ± SD (n = 3). Statistical significance was determined using unpaired t-test on GraphPad InStat v. 3.06 ($p < 0.05$ was-considered statistically significant).

3. Results and discussion

3.1. HPLC method for DOX

We developed and validated the analytical method for the estimation of DOX by HPLC with PDA detector. The HPLC chromatogram of DOX showed that DOX was eluted from the column at a retention time (R_t) of 9.778 ± 0.001 min (Fig. 1(A)). The standard calibration curve of DOX displayed a linear relationship in the tested range of 1–100 μg mL^{-1} with the coefficient of correlation value, $R^2 = 0.9993$ (n = 3), as shown in Fig. 1(B).

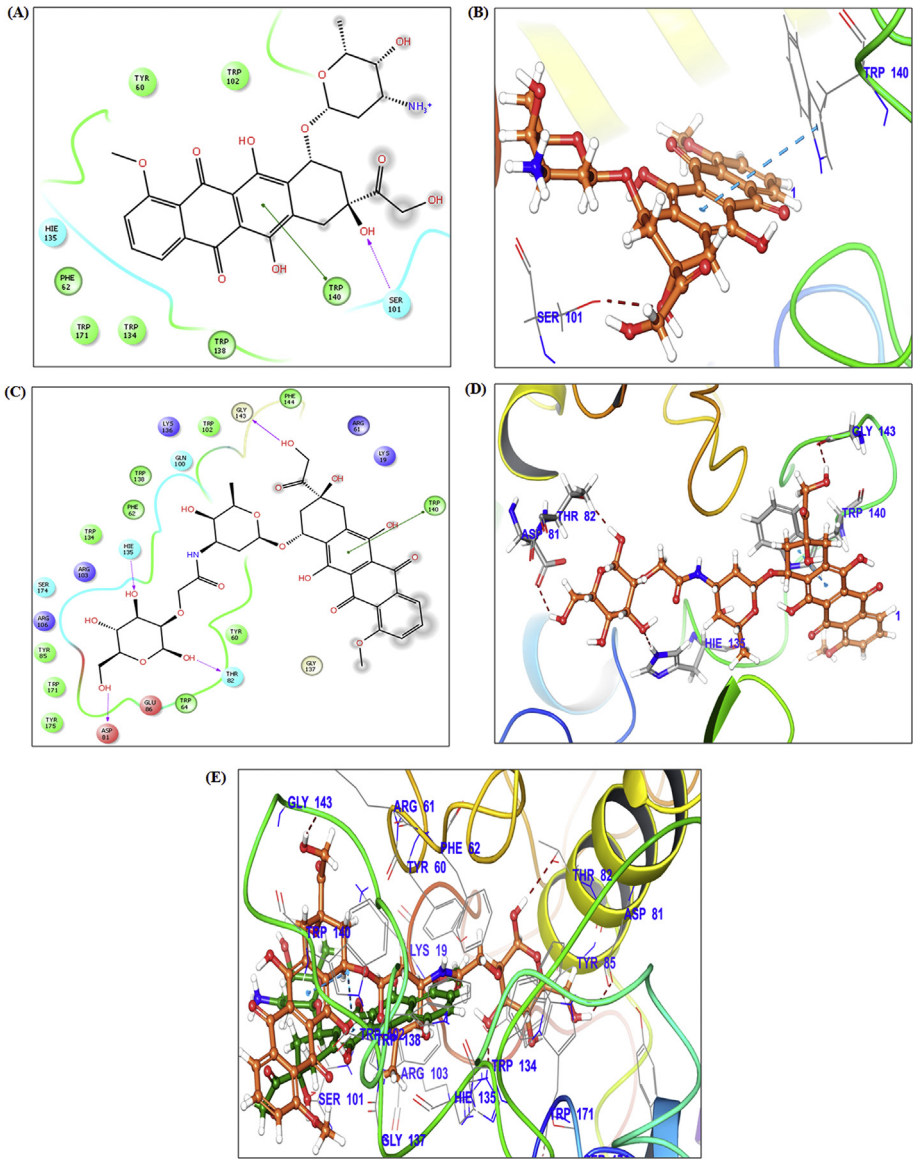

Fig. 9. Best conformations for compounds docked to FRA (green color) (A) Ligplot of DOX (B) 3D plots showing binding sites of DOX (grey sticks) with the corresponding FRA (C) Ligplot of DOX-CM-ABRS SPIONs (D) 3D plots showing binding sites of DOX-CM-ABRS SPIONs (grey sticks) with the corresponding FRA, and (E) Superimposition of DOX-CM-ABRS SPIONs (brown) at catalytic domain of FRA with DOX (blue).

3.2. Preparation of DOX-CM-ABRS SPIONs

3.2.1. Synthesis of CM-ABRS

Carboxymethylation process was found to improve the physicochemical properties of native ABRS with an optimum degree of substitution (DS) of 1.23. This fact was further confirmed by FT-IR and NMR spectra (H^1 and C^{13}) of CM-ABRS, as described in our previous work (Mohapatra et al., 2017). CM-ABRS acts as a potential stabilizing agent for synthesis of SPIONs, due to the presence of numerous carboxyl (-COOH) and hydroxyl (-OH) groups.

3.2.2. Synthesis of CM-ABRS SPIONs

Stable CM-ABRS SPIONs synthesized by using optimum concentration of CM-ABRS (0.8% (w/v)) were more refined by using homogenizer. CM-ABRS is supposed to interact with cationic iron by donating a lone pair of electrons present on the surface of iron oxide (magnetite) through Lewis acid-base reaction (Laurent et al., 2008). The optimized CM-ABRS (0.8% (w/v)) SPIONs were centrifuged (High-Speed Refrigerated Micro Centrifuge; MX-305; Tomy, Japan) at 14,500 rpm for 30 min at 4°C prior to lyophilization process (with mannitol) in a freeze dryer (Labconco, USA) at -58.7°C and 13 mTorr. The lyophilized CM-ABRS (0.8% (w/v)) SPIONs were kept in tightly closed container for future use, as described in our previous study (Mohapatra et al., 2018).

3.2.3. DOX loading onto CM-ABRS SPIONs

The loading capacity of CM-ABRS (0.8% (w/v)) SPIONs was estimated by observing fluorescence quenching occurring due to intermolecular interactions between constant amount of DOX in solution with variable concentrations of CM-ABRS (0.8% (w/v)) SPIONs. DOX was loaded onto CM-ABRS (0.8% (w/v)) SPIONs by electrostatic interactions between them, as depicted in Fig. 2(A), which is in accordance with the previous hypothesis reported for incorporation of cationic drugs (DOX) onto anionic polymers (Park et al., 2012; Wang et al., 2015; Zhang et al., 2018b). Sequential decreases in the intensity of native fluorescence spectrum of DOX were monitored as the increasing amounts of CM-ABRS (0.8% (w/v)) SPIONs were added to it, as shown in Fig. 2(B). The maximal quenching of DOX fluorescence was achieved with approximately120 μg of DOX to 2.0 mg of CM-ABRS (0.8% (w/v)) SPIONs,

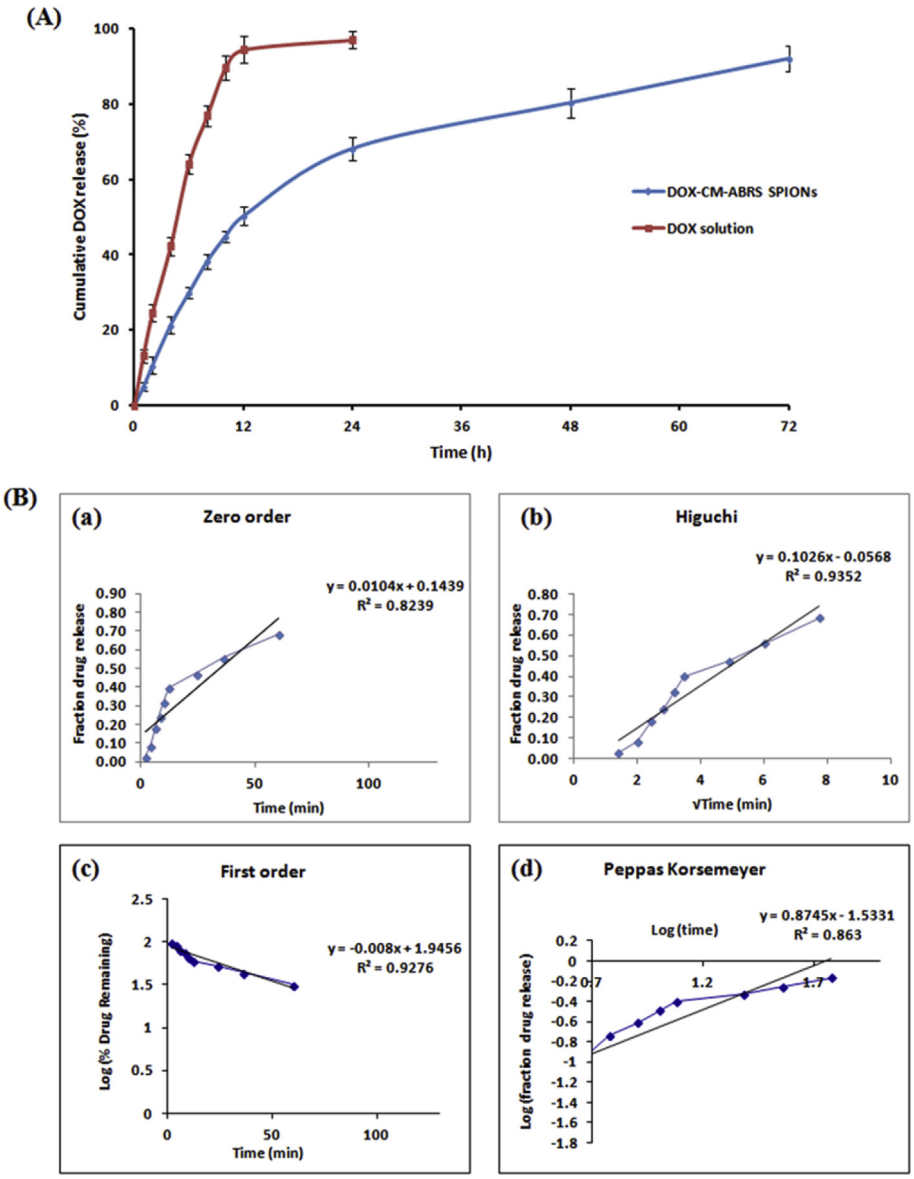

Fig. 10. (A) *In vitro* cumulative drug release profile of DOX solution and DOX-CM-ABRS (0.8% (w/v)) SPIONs in PBS (pH 7.4) at 37°C, and (B) Release kinetics modeling: Release pattern graphs of DOX-CM-ABRS (0.8% (w/v)) SPIONs applying various kinetic models (Data presented as mean ± SD (n = 3).

representing that the optimal loading amount of DOX to CM-ABRS (0.8% (w/v)) SPIONs is about 6 % (w/w), i. e, the formulation dc7. On further increasing the concentration of CM-ABRS (0.8% (w/v)) SPIONs, no change in fluorescence quenching was noticed, as shown in Fig. 2(B). DOX loading and entrapment efficiency in the final optimized formulation (dc7), were found to be 6.0 ± 0.3% (w/w) and 90.24 ± 0.8%, respectively. Due to tunable properties and ability for electrostatic interaction with cationic drug molecule, CM-ABRS can serve as a potential carrier for drug delivery with the advantage of high loading capacity and controlled release of drug molecules (Ispas-Szabo et al., 2017; Mohapatra et al., 2017; Wang et al., 2011).

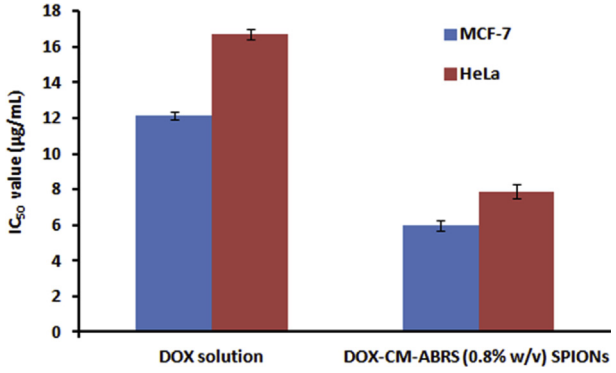

Fig. 11. Comparative antiproliferative effect (IC_{50}) of DOX solution and DOX-CM-ABRS SPIONs (0.8% (w/v)) on MCF-7 and HeLa cell lines (Data presented as mean ± SD (n=3).

3.3. Physicochemical characterization of DOX-CM-ABRS SPIONs

3.3.1. Particle size, size distribution and surface charge: DLS analysis

Particle size for DOX-CM-ABRS (0.8% (w/v)) SPIONs was found to be 205.6 ± 0.211 nm with PDI of 0.380 ± 0.015 by DLS, as shown in Fig. 3(A). There was no appreciable change in Z-average of DOX-CM-ABRS (0.8% (w/v)) SPIONs after DOX loading, as compared to CM-ABRS SPIONs (0.8% (w/v)) (201.0 ± 1.32 nm; PDI = 0.308 ± 0.020) by using 5% (w/v) mannitol as a cryoprotectant after reconstitution. The surface charge of CM-ABRS SPIONs (0.8% (w/v)), employing Zetasizer

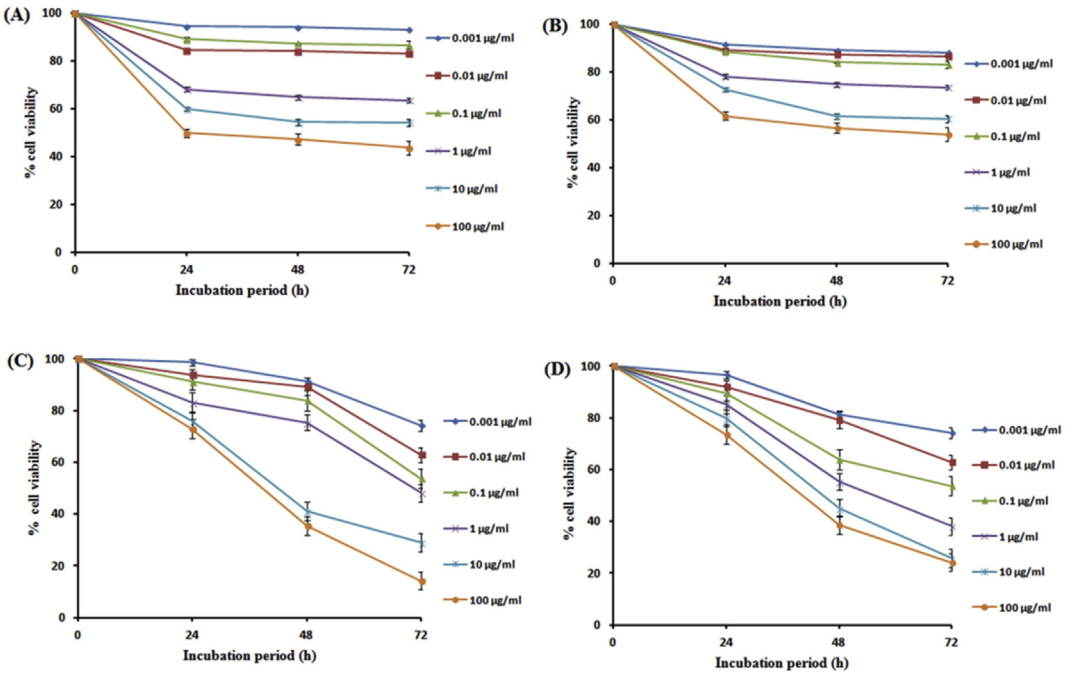

Fig. 12. Comparative cell viability of (A) MCF-7 (B) HeLa cell lines after exposure to 0.1–100 μg mL^{-1} DOX solution, and comparative viability of (C) MCF-7 (D) HeLa cell lines after exposure to 0.1–100 μg mL^{-1} equivalent of DOX concentration for DOX-CM-ABRS (0.8% (w/v)) SPIONs.

was found to be -28.2 mV, while that for DOX- CM-ABRS SPIONs (0.8% (w/v)) was found to be -26.1 mV, as shown in Fig. 3(B), respectively. A high absolute value of ZP (>25 mV) suggests good colloidal stability of nanocarriers (Xu, 2001).

The negative zeta potential for CM-ABRS (0.8% (w/v)) SPIONs can be attributed to the presence of carboxyl and hydroxyl groups on the CM-ABRS molecules, used for the stabilization of SPIONs (Mallick et al., 2015). The decrease in absolute value of zeta potential in case of DOX-CM-ABRS (0.8% (w/v)) SPIONs can be because of the neutralization of surface charge of CM-ABRS molecules, due to the charge complexation effect (Kumar et al., 2016). From this study, the DOX-CM-ABRS (0.8% (w/v)) SPIONs were found to be colloidally stable in nano-metric range for *in vivo* studies.

3.3.2. Particle morphology: transmission electron microscopy

The TEM micrographs of CM-ABRS (0.8% (w/v)) SPIONs and DOX-CM-ABRS (0.8% (w/v)) SPIONs, shown in Fig. 4(A) and (B), respectively, revealed the presence of spherical nano-sized particles with an average diameter around ~200 nm (Couvreur et al., 1995). As observed from the TEM images, there was no considerable increase in size of the particles upon DOX loading. CM-ABRS being polymeric in nature and having multiple hydroxyl and carboxyl groups showed multiple iron oxide cores trapped in a single cluster Fig. 4(C) (Amstad et al., 2011; Mallick et al., 2015).

3.3.3. Interaction of CM-ABRS SPIONs with DOX: fourier-transform infrared (FT-IR) spectroscopy

The FT-IR spectra for CM-ABRS (0.8% (w/v)) SPIONs, DOX and DOX-CM-ABRS (0.8% (w/v)) SPIONs are shown in Fig. 5. The nature of interaction of pristine magnetite with CM-ABRS in the final formulation (CM-ABRS (0.8% (w/v)) SPIONs) as shown in Fig. 5(A) was studied in our previous work (Mohapatra et al., 2018). Hence, we focused on the nature of interaction of DOX with CM-ABRS (0.8% (w/v)) SPIONs extensively. The bands observed at 804 cm^{-1} due to N–H wag and that at 1581 and 1616 cm^{-1} due to N–H scissoring in pure DOX diminished in the FT-IR spectrum of DOX-CM-ABRS (0.8% (w/v)) SPIONs, as depicted in Fig. 5(B). It confirmed that the attachment of DOX to the CM-ABRS (0.8% (w/v)) SPIONs, occurs via the interaction of $–NH_2$ and –OH groups of DOX with –OH groups of CM-ABRS through hydrogen bonding which is consistent with a previous research work (Kayal & Ramanujan, 2010). Also, the carboxylate asymmetric stretching vibration which appeared in CM-ABRS (0.8% (w/v)) SPIONs, at 1638 cm^{-1} was shifted to 1641 cm^{-1} in case of DOX-CM-ABRS (0.8% (w/v)) SPIONs, indicating that the NH_2 group in DOX has interacted with the carboxylate groups in the structure of CM-ABRS (Fig. 5(C)). Thus, binding of DOX with CM-ABRS SPIONs, can be attributed to the interaction of amine group of DOX with hydroxyl groups on the sugar backbone of CM-ABRS via hydrogen bonding and to the carboxylate groups of CM-ABRS via electrostatic interactions, which is consistent with a previous study (Reyes-Ortega et al., 2017).

3.3.4. Crystallographic properties: X-Ray diffraction

The XRD-diffractogram of DOX-CM-ABRS (0.8% (w/v)) SPIONs showed results similar to similar to that of CM-ABRS (0.8% (w/v)) SPIONs (Fig. 6(A)). There was no noticeable change in crystalline nature of CM-ABRS SPIONs after DOX loading, as shown in Fig. 6(B). It indicates that magnetite core of SPIONs consisted of cubic phase Fe_3O_4 and there was no interference in crystal form of magnetite as was observed in the final formulation DOX-CM-ABRS (0.8% (w/v)) SPIONs, due to surface coating and drug loading. The broadening of peaks observed in case of DOX-CM-ABRS (0.8% (w/v)) SPIONs as compared to pristine iron oxide, may be due to decrease in crystallite size, which is in accordance with previous reports, indicating peak broadening with increasing polymer concentration around iron oxide core (Kayal & Ramanujan, 2010).

3.3.5. Magnetic properties measurement: vibration sample magnetometry (VSM)

The magnetic properties of CM-ABRS (0.8% (w/v)) SPIONs and DOX-CM-ABRS (0.8% (w/v)) SPIONs were confirmed by vibrating sample magnetometry (VSM), by plotting magnetization versus magnetic field (M–H loop) curve at room temperature, as illustrated in Fig. 7(A) and (B) respectively. In the hysteresis M-H curves, presence of almost super-imposible upward and downward segments proved that the formulations were superparamagnetic in nature with very small magnetite core. There was a major difference observed in the value of saturation magnetization (M_s) for CM-ABRS SPIONs (33.688 emu g^{-1}) as compared to DOX-CM-

ABRS SPIONs (4.259 emu g^{-1}) after drug loading. This might be due to the presence of non-magnetic component DOX on to the surface of CM-ABRS SPIONs, which contributed to a decrease in the overall super-paramagnetic iron oxide content (Gomez-Lopera et al., 2001; Li et al., 2011; Yu et al., 2008). Furthermore, DOX-CM-ABRS SPIONs could be separated quickly and easily from the solution when using the magnet, thus facilitating the delivery of drug at the target site upon application of the external magnetic field.

3.4. In silico drug design study: molecular docking

Modeling studies play an important role in order to construct molecular models that incorporate all experimental evidences reported. These models are necessary to obtain a consistent and more precise picture of the biologically-active molecules at the atomic level and furthermore, provide new insights that can be used to design novel therapeutic agents (Agudelo et al., 2014). The molecular docking study of DOX-CM-ABRS SPIONs against HER-2 Protein receptor (Organism: human) and FRA, revealed a common binding orientation of DOX-CM-ABRS SPIONs in the catalytic binding pocket of HER-2 Protein receptor (PDBID: 5jeb).

Herein, we report the binding pose of DOX and DOX-CM-ABRS SPIONs with HER-2 Protein and FRA, as shown in the form of ligplots depicted in Fig. 8(A) and (C), and Fig. 9(A) and (C), respectively. Binding interaction of DOX and DOX-CM-ABRS SPIONs with backbone of HER-2 Protein receptor with Glu 738, Leu764, Met 769 and Asn 972 was studied as 3D plots shown in Figs. 8(B) and (D) and for FRA receptor with Gln143, Asp81, Thr82 and His135 and pi-pi stacking with Trp143, shown as 3D plots in Figs. 9(B) and (D), respectively. On superimposing the DOX-CM-ABRS SPIONs with DOX in catalytic domain of HER-2 Protein receptor (Fig. 8(E)), it was found to have a similar interaction, but with better docking score for DOX-CM-ABRS SPIONs (-13.396) as compared to standard DOX (-12.537). Similarly, in case of FRA receptor (Fig. 9(E)) better docking score was observed for DOX-CM-ABRS SPIONs (-11.388) as compared to standard DOX (-6.675). The RMSD between co-crystal and re-docked poses was found to be 0.331 (<2A°), which confirmed the validity of the docking parameters (Paul and Mukhopadhyay, 2004). These results indicated the high accuracy of the Auto Dock simulation in comparison with biological methods.

3.5. In vitro drug release profile

The *In vitro* release of DOX from DOX-CM-ABRS (0.8% (w/v)) SPIONs at pH 7.4 was compared with standard DOX solution under the same experimental condition as shown in Fig. 10(A). DOX solution released 90% of the cumulative DOX within a period of 10 h, whereas DOX-CM-ABRS (0.8% (w/v)) SPIONs released approximately 10.6% in the first 2 h without an initial burst release, followed by a 68.23% of cumulative DOX release within 24 h. The drug release profile of DOX-CM-ABRS (0.8% (w/v)) SPIONs followed a steady rate, lasting up to 72 h (Fig. 10(A)), which could be explained by the slow diffusion of the drug molecule through the polymeric matrix (Duncan, 1999; Park et al., 2012).

The release pattern exhibited by DOX-CM-ABRS (0.8% (w/v)) SPIONs followed Higuchi model with regression coefficient (R^2) value of 0.9352, as shown in Fig. 10(B). This sustained release behavior of DOX-CM-ABRS (0.8% (w/v)) SPIONs might make it a high potential candidate for controlled drug delivery system by maintaining the therapeutic level for a longer time as compared to free DOX solution (Agrawal, Sanabria-DeLong, Coburn, Tew & Bhatia, 2006; Guo et al., 2010; Liechty et al., 2010).

3.6. In vitro cell viability assay

Cytotoxicity effect of DOX solution and DOX-CM-ABRS (0.8% (w/v)) SPIONs was studied on MCF-7 and HeLa cell lines and expressed in terms of IC_{50} values, as shown in Fig. 11. IC_{50} value for DOX solution was found to be 12.126 ± 0.210 μg mL^{-1} as compared to DOX-CM-ABRS (0.8% (w/v)) SPIONs (5.946 ± 0.137 μg mL^{-1}) for MCF-7 cell lines. On the other hand, IC_{50} value for DOX solution was found to be 16.716 ± 0.301 μg mL^{-1} as compared to DOX-CM-ABRS (0.8% (w/v)) SPIONs (7.894 ± 0.428 μg mL^{-1}) for HeLa cell lines. This difference in IC_{50} values against both the cell lines concluded increased anti-proliferative efficacy of DOX-CM-ABRS (0.8% (w/v)) SPIONs over DOX ($p < 0.0001$), may be due to endocytosis of drug-loaded SPIONs and subsequent release of drug inside the cells (Thi et al., 2019; Zhu et al., 2013). The differences were statistically significant ($p < 0.0001$) as determined by unpaired *t-test* (GraphPad InStat v. 3.06).

DOX solution exhibited characteristic dose-response curves for both MCF-7 and HeLa cell lines (Fig. 12(A) and (B)) which show an initial steep decline in cell survival in the initial incubation period of 24 h for all the tested concentrations and very little cytotoxicity was observed after the incubation period of 48 and 72 h.

Enhanced cytotoxicity in both the cell lines was observed for DOX-CM-ABRS (0.8% (w/v)) SPIONs (Fig. 12(C) and (D)), after the incubation period of 48 and 72 h as compared to 24 h, which might be attributed to slow release of entrapped drug from the polymeric matrix and favoring drug efflux into the cells by creating concentration gradient (Jain et al., 2012). Another factor may be the internalization of SPIONs and release of drug in the interior part of the cells (Schöpf et al., 2005; Wilhelm et al., 2003).

Hence, DOX-CM-ABRS (0.8% (w/v)) SPIONs were found to have potent dose-dependent and time-dependent cytotoxicity as compared to DOX solution (which showed only dose-dependent cytotoxicity on both MCF-7 and HeLa cell lines) (Akbarzadeh et al., 2012).

4. Conclusion

4.1. Future perspective

Super paramagnetic iron oxide nanoparticles (SPIONs), have been widely used in medicine for drug delivery, diagnostic imaging, and therapeutic applications owing to their nontoxic, biodegradable, and inexpensive in nature. In addition, SPIONs are FDA-approved biocompatible materials and can be cleared from the body via the iron metabolic pathway.

The CM-ABRS stabilized SPIONs were chemically synthesized and successfully loaded with water-soluble cationic DOX via electrostatic interaction. These nanohybrids had excellent water dispersibility, colloidal stability, and sustained release pattern of drug from the polymeric matrix, and can be used in chemotherapy as delivery vectors for chemotherapeutic drugs. MTT assay on human breast cancer (MCF-7) and cervical cancer (HeLa) cell lines showed statistically-significant decrease ($p < 0.0001$) in IC_{50} values for DOX-CM-ABRS (0.8% (w/v)) SPIONs as compared to standard DOX solution. Further, drug design study (molecular docking) against HER-2 and FRA receptors conferred that DOX-CM-ABRS (0.8% (w/v)) SPIONs showed better interaction at the molecular level after administration, as compared to standard DOX solution. Summarizing the results of the experiments, one can conclude that the synthesized DOX-CM-ABRS (0.8% (w/v)) SPIONs could act as appropriate and efficient candidates for cancer management. Future work will include an *in vivo* investigation of the targeting ability and effectiveness of DOX-CM-ABRS (0.8% (w/v)) SPIONs in the treatment of tumor for translation to clinical applications.

Declarations

Author contribution statement

Sharmistha Mohapatra, Mohammed Asfer, Mohammed Anwar, Kalicharan Sharma, Mymoona Akhter, Farhan Jalees Ahmad and Anees Ahmad Siddiqui: Conceived and designed the experiments; Performed

the experiments; Analyzed and interpreted the data; Contributed reagents, materials, analysis tools or data; Wrote the paper.

Funding statement

This work was supported by the Indian Council of Medical Research (ICMR), India grant of senior research fellowship (Grant No. 45/36/2014-Nan/BMS).

Competing interest statement

The authors declare no conflict of interest.

Additional information

No additional information is available for this paper.

Acknowledgements

Authors are also thankful to Sophisticated Analytical Instrumentation Facility (SAIF), AIIMS, New Delhi, India, for carrying out the TEM analysis of samples.

References

Agrawal, S.K., Sanabria-DeLong, N., Coburn, J.M., Tew, G.N., Bhatia, S.R., 2006. Novel drug release profiles from micellar solutions of PLA–PEO–PLA triblock copolymers. J. Control. Release 112 (1), 64–71.

Agudelo, D., Bourassa, P., Bérubé, G., Tajmir-Riahi, H.-A., 2014. Intercalation of antitumor drug doxorubicin and its analogue by DNA duplex: structural features and biological implications. Int. J. Biol. Macromol. 66, 144–150.

Ahmad, M.Z., Akhter, S., Ahmad, I., Singh, A., Anwar, M., Shamim, M., Ahmad, F.J., 2012. *In vitro* and in vivo evaluation of Assam Bora rice starch-based bioadhesive microsphere as a drug carrier for colon targeting. Expert Opin. Drug Deliv. 9 (2), 141–149.

Akbarzadeh, A., Mikaeili, H., Zarghami, N., Mohammad, R., Barkhordari, A., Davaran, S., 2012. Preparation and *In vitro* evaluation of doxorubicin-loaded Fe3O4 magnetic nanoparticles modified with biocompatible copolymers. Int. J. Nanomed. 7, 511.

Amstad, E., Textor, M., Reimhult, E., 2011. Stabilization and functionalization of iron oxide nanoparticles for biomedical applications. Nanoscale 3 (7), 2819–2843.

Arruebo, M., Fernández-Pacheco, R., Ibarra, M.R., Santamaría, J., 2007. Magnetic nanoparticles for drug delivery. Nano Today 2 (3), 22–32.

Chen, J., Ding, J., Xu, W., Sun, T., Xiao, H., Zhuang, X., Chen, X., 2017. Receptor and microenvironment dual-recognizable nanogel for targeted chemotherapy of highly metastatic malignancy. Nano Lett. 17 (7), 4526–4533.

Cheng, K., Peng, S., Xu, C., Sun, S., 2009. Porous hollow Fe3O4 nanoparticles for targeted delivery and controlled release of cisplatin. J. Am. Chem. Soc. 131 (30), 10637–10644.

Corot, C., Robert, P., Idée, J.-M., Port, M., 2006. Recent advances in iron oxide nanocrystal technology for medical imaging. Adv. Drug Deliv. Rev. 58 (14), 1471–1504.

Couvreur, P., Dubernet, C., Puisieux, F., 1995. Controlled drug delivery with nanoparticles: current possibilities and future trends. Eur. J. Pharm. Biopharm. 41 (1), 2–13.

Duncan, R., 1999. Polymer conjugates for tumour targeting and intracytoplasmic delivery. The EPR effect as a common gateway? Pharmaceut. Sci. Technol. Today 2 (11), 441–449.

Fang, C., Bhattarai, N., Sun, C., Zhang, M., 2009. Functionalized nanoparticles with long-term stability in biological media. Small 5 (14), 1637–1641.

Friesner, R.A., Murphy, R.B., Repasky, M.P., Frye, L.L., Greenwood, J.R., Halgren, T.A., Sanschagrin, P.C., Mainz, D.T., 2006. Extra precision glide: docking and scoring incorporating a model of hydrophobic enclosure for protein − ligand complexes. J. Med. Chem. 49 (21), 6177–6196.

Gomez-Lopera, S., Plaza, R., Delgado, A., 2001. Synthesis and characterization of spherical magnetite/biodegradable polymer composite particles. J. Colloid Interface Sci. 240 (1), 40–47.

Guo, M., Yan, Y., Liu, X., Yan, H., Liu, K., Zhang, H., Cao, Y., 2010. Multilayer nanoparticles with a magnetite core and a polycation inner shell as pH-responsive carriers for drug delivery. Nanoscale 2 (3), 434–441.

Hoke, E.M., Maylock, C.A., Shacter, E., 2005. Desferal inhibits breast tumor growth and does not interfere with the tumoricidal activity of doxorubicin. Free Radic. Biol. Med. 39 (3), 403–411.

Ispas-Szabo, P., De Koninck, P., Calinescu, C., Mateescu, M.A., 2017. Carboxymethyl starch excipients for drug chronodelivery. AAPS Pharm. Sci. Tech. 18 (5), 1673–1682.

Jain, V., Swarnakar, N.K., Mishra, P.R., Verma, A., Kaul, A., Mishra, A.K., Jain, N.K., 2012. Paclitaxel loaded PEGylated gleceryl monooleate based nanoparticulate carriers in chemotherapy. Biomaterials 33 (29), 7206–7220.

Jones, G., Willett, P., Glen, R.C., Leach, A.R., Taylor, R., 1997. Development and validation of a genetic algorithm for flexible docking. J. Mol. Biol. 267 (3), 727–748.

Kayal, S., Ramanujan, R., 2010. Doxorubicin loaded PVA coated iron oxide nanoparticles for targeted drug delivery. Mater. Sci. Eng. C 30 (3), 484–490.

Kim, D.K., Mikhaylova, M., Wang, F.H., Kehr, J., Bjelke, B., Zhang, Y., Tsakalakos, T., Muhammed, M., 2003. Starch-coated superparamagnetic nanoparticles as MR contrast agents. Chem. Mater. 15 (23), 4343–4351.

Kumar, P., Agnihotri, S., Roy, I., 2016. Synthesis of dox drug conjugation and citric acid stabilized superparamagnetic iron-oxide nanoparticles for drug delivery. Biochem. Physiol. 5 (194), 2.

Lammers, T., Kiessling, F., Hennink, W.E., Storm, G., 2010. Nanotheranostics and image-guided drug delivery: current concepts and future directions. Mol. Pharm. 7 (6), 1899–1912.

Laurent, S., Forge, D., Port, M., Roch, A., Robic, C., Vander Elst, L., Muller, R.N., 2008. Magnetic iron oxide nanoparticles: synthesis, stabilization, vectorization, physicochemical characterizations, and biological applications. Chem. Rev. 108 (6), 2064–2110.

Laurent, S., Saei, A.A., Behzadi, S., Panahifar, A., Mahmoudi, M., 2014. Superparamagnetic iron oxide nanoparticles for delivery of therapeutic agents: opportunities and challenges. Expert Opin. Drug Deliv. 11 (9), 1449–1470.

Li, F., Sun, J., Zhu, H., Wen, X., Lin, C., Shi, D., 2011. Preparation and characterization novel polymer-coated magnetic nanoparticles as carriers for doxorubicin. Colloids Surfaces B Biointerfaces 88 (1), 58–62.

Liechty, W.B., Kryscio, D.R., Slaughter, B.V., Peppas, N.A., 2010. Polymers for drug delivery systems. Annu. Rev. Chem. Biomol. Eng. 1, 149–173.

Mallick, N., Anwar, M., Asfer, M., Mehdi, S.H., Rizvi, M.M.A., Panda, A.K., Talegaonkar, S., Ahmad, F.J., 2016. Chondroitin sulfate-capped super-paramagnetic iron oxide nanoparticles as potential carriers of doxorubicin hydrochloride. Carbohydr. Polym. 151, 546–556.

Mallick, N., Asfer, M., Anwar, M., Kumar, A., Samim, M., Talegaonkar, S., Ahmad, F.J., 2015. Rhodamine-loaded, cross-linked, carboxymethyl cellulose sodium-coated super-paramagnetic iron oxide nanoparticles: development and *In vitro* localization study for magnetic drug-targeting applications. Colloid. Surf. Physicochem. Eng. Asp. 481, 51–62.

Meka, V.S., Sing, M.K., Pichika, M.R., Nali, S.R., Kolapalli, V.R., Kesharwani, P., 2017. A comprehensive review on polyelectrolyte complexes. Drug Discov. Today 22 (11), 1697–1706.

Ménard, S., Pupa, S.M., Campiglio, M., Tagliabue, E.J.O., 2003. Biologic and therapeutic role of HER2 in cancer. Oncogene 22, 6570.

Mohapatra, S., Asfer, M., Anwar, M., Ahmed, S., Ahmad, F.J., Siddiqui, A.A., 2018. Carboxymethyl Assam Bora rice starch coated SPIONs: synthesis, characterization and *In vitro* localization in a micro capillary for simulating a targeted drug delivery system. Int. J. Biol. Macromol. 115, 920–932.

Mohapatra, S., Siddiqui, A.A., Anwar, M., Bhardwaj, N., Akhter, S., Ahmad, F.J., 2017. Synthesis and characterization of novel carboxymethyl Assam Bora rice starch for the controlled release of cationic anticancer drug based on electrostatic interactions. AAPS PharmSciTech 1–14.

Neve, R., Lane, H., Hyne, N., 2001. The role of overexpressed HER2 in transformation. J. Ann. Oncol. 12 (suppl_1), S9–S13.

Olayioye, M.A., 2001. Intracellular signaling pathways of ErbB2/HER-2 and family members. J. Breast Cancer Res. 3 (6), 385.

Park, J.H., von Maltzahn, G., Zhang, L., Schwartz, M.P., Ruoslahti, E., Bhatia, S.N., Sailor, M.J., 2008. Magnetic iron oxide nanoworms for tumor targeting and imaging. Adv. Mater. 20 (9), 1630–1635.

Park, S., Kim, H.S., Kim, W.J., Yoo, H.S., 2012. Pluronic@ Fe3O4 nanoparticles with robust incorporation of doxorubicin by thermo-responsiveness. Int. J. Pharm. 424 (1-2), 107–114.

Paul, M.K., Mukhopadhyay, A.K., 2004. Tyrosine kinase–role and significance in cancer. Int. J. Med. Sci. 1 (2), 101.

Pharmacopoeia, B., 1999. The Department of Health. British Pharmacopoeia Commission. The Stationary Office, London.

Release, S., 2017. QikProp, 2. Schrödinger, LLC, New York, NY, USA.

Reyes-Ortega, F., Delgado, Á., Schneider, E., Checa Fernández, B., Iglesias, G., 2017. Magnetic nanoparticles coated with a thermosensitive polymer with hyperthermia properties. Polymers 10 (1), 10.

Saboktakin, M.R., Maharramov, A., Ramazanov, M.A., 2009. Synthesis and characterization of superparamagnetic nanoparticles coated with carboxymethyl starch (CMS) for magnetic resonance imaging technique. Carbohydr. Polym. 78 (2), 292–295.

Schöpf, B., Neuberger, T., Schulze, K., Petri, A., Chastellain, M., Hofmann, M., Hofmann, H., Von Rechenberg, B., 2005. Methodology description for detection of cellular uptake of PVA coated superparamagnetic iron oxide nanoparticles (SPION) in synovial cells of sheep. J. Magn. Magn. Mater. 293 (1), 411–418.

Shubayev, V.I., Pisanic II, T.R., Jin, S., 2009. Magnetic nanoparticles for theragnostics. Adv. Drug Deliv. Rev. 61 (6), 467–477.

Tang, H., Zhao, W., Yu, J., Li, Y., Zhao, C., 2019. Recent development of pH-responsive polymers for cancer nanomedicine. Molecules 24 (1), 4.

Thi, H., Thanh, T., Nguyen Tran, D.-H., Bach, L.G., Vu-Quang, H., Nguyen, D.C., Park, K.D., Nguyen, D.H., 2019. Functional magnetic core-shell system-based iron oxide nanoparticle coated with biocompatible copolymer for anticancer drug delivery. Pharmaceutics 11 (3), 120.

Veiseh, O., Gunn, J.W., Zhang, M., 2010. Design and fabrication of magnetic nanoparticles for targeted drug delivery and imaging. Adv. Drug Deliv. Rev. 62 (3), 284–304.

Wang, Y., Assaad, E., Ispas-Szabo, P., Mateescu, M., Zhu, X., 2011. NMR imaging of chitosan and carboxymethyl starch tablets: swelling and hydration of the polyelectrolyte complex. Int. J. Pharmaceutics 419 (1-2), 215–221.

Wang, J., Xu, W., Guo, H., Ding, J., Chen, J., Guan, J., Wang, C., 2015. Selective intracellular drug delivery from pH-responsive polyion complex micelle for enhanced malignancy suppression in vivo. Colloids Surfaces B Biointerfaces 135, 283–290.

Wilhelm, C., Billotey, C., Roger, J., Pons, J., Bacri, J.-C., Gazeau, F., 2003. Intracellular uptake of anionic superparamagnetic nanoparticles as a function of their surface coating. Biomaterials 24 (6), 1001–1011.

Xiao, H., Stefanick, J.F., Jia, X., Jing, X., Kiziltepe, T., Zhang, Y., Bilgicer, B., 2013. Micellar nanoparticle formation via electrostatic interactions for delivering multinuclear platinum (II) drugs. Chem. Commun. 49 (42), 4809–4811.

Xie, J., Huang, J., Li, X., Sun, S., Chen, X., 2009. Iron oxide nanoparticle platform for biomedical applications. Curr. Med. Chem. 16 (10), 1278–1294.

Xu, R., 2001. Particle Characterization: Light Scattering Methods. Springer Science & Business Media.

Xu, W., Ding, J., Chen, X., 2017. Reduction-responsive polypeptide micelles for intracellular delivery of antineoplastic agent. Biomacromolecules 18 (10), 3291–3301.

Yu, M.K., Jeong, Y.Y., Park, J., Park, S., Kim, J.W., Min, J.J., Kim, K., Jon, S., 2008. Drug-loaded superparamagnetic iron oxide nanoparticles for combined cancer imaging and therapy in vivo. Angew. Chem. Int. Ed. 47 (29), 5362–5365.

Zhang, Q., Ding, J., Lv, C., Xu, W., Sun, X., Meng, X., 2015. Epirubicin-complexed polypeptide micelle effectively and safely treats hepatocellular carcinoma. Polymers 7 (11), 2410–2430.

Zhang, Y., Cai, L., Li, D., Lao, Y.-H., Liu, D., Li, M., Ding, J., Chen, X., 2018a. Tumor microenvironment-responsive hyaluronate-calcium carbonate hybrid nanoparticle enables effective chemotherapy for primary and advanced osteosarcomas. Nano Res. 11, 4806–4822.

Zhang, Y., Wang, F., Li, M., Yu, Z., Qi, R., Ding, J., Zhang, Z., Chen, X., 2018b. Self-stabilized hyaluronate nanogel for intracellular codelivery of doxorubicin and cisplatin to osteosarcoma. Adv. Sci. 5 (5), 1700821.

Zhu, L., Wang, T., Perche, F., Taigind, A., Torchilin, V.P., 2013. Enhanced anticancer activity of nanopreparation containing an MMP2-sensitive PEG-drug conjugate and cell-penetrating moiety. Proc. Natl. Acad. Sci. Unit. States Am. 110 (42), 17047–17052.